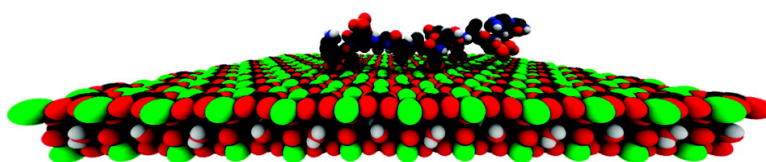Article

Control of Calcium Oxalate Crystal Growth by Face-Specific Adsorption of an Osteopontin Phosphopeptide

Bernd Grohe, Jason O'Young, D. Andrei Ionescu, Gilles Lajoie, Kem A. Rogers, Mikko Karttunen, Harvey A. Goldberg, and Graeme K. Hunter

More About This Article

Additional resources and features associated with this article are available within the HTML version:

- Supporting Information
- Links to the 3 articles that cite this article, as of the time of this article download
- Access to high resolution figures
- Links to articles and content related to this article
- Copyright permission to reproduce figures and/or text from this article

View the Full Text HTML

J|A|C|S

A R T I C L E S

Control of Calcium Oxalate Crystal Growth by Face-Specific Adsorption of an Osteopontin Phosphopeptide

Bernd Grohe,[†] Jason O'Young,[†,‡] D. Andrei Ionescu,[†,⊥] Gilles Lajoie,[‡] Kem A. Rogers,[§] Mikko Karttunen,[∥] Harvey A. Goldberg,[†,‡] and Graeme K. Hunter*,[†,‡]

Contribution from the CIHR Group in Skeletal Development and Remodeling, School of Dentistry, Department of Biochemistry, Department of Anatomy and Cell Biology, and Department of Applied Mathematics, University of Western Ontario, London, Canada

Received June 21, 2007; E-mail: graeme.hunter@schulich.uwo.ca

Abstract: Mineral-associated proteins have been proposed to regulate many aspects of biomineralization, including the location, type, orientation, shape, and texture of crystals. To understand how proteins achieve this exquisite level of control, we are studying the interaction between the phosphoprotein osteopontin (OPN) and the biomineral calcium oxalate monohydrate (COM). In the present study, we have synthesized peptides corresponding to amino acids 220−235 of rat bone OPN (pSHEpSTEQSDAIDpSAEK), one of several highly phosphorylated, aspartic-, and glutamic acid-rich sequences found in the protein. To investigate the role of phosphorylation in interaction with crystals, peptides containing no (P0), one (P1), or all three (P3) phosphates were prepared. Using a novel combination of confocal microscopy and scanning electron microscopy, we show that these peptides adsorb preferentially to {100} faces of COM and inhibit growth of these faces in a phosphorylation-dependent manner. To characterize the mechanism of adsorption of OPN peptides to COM, we have performed the first atomic-scale molecular-dynamics simulation of a protein−crystal interaction. P3 adsorbs to the {100} face much more rapidly than P1, which in turn adsorbs more rapidly than P0. In all cases, aspartic and glutamic acid, not phosphoserine, are the amino acids in closest contact with the crystal surface. These studies have identified a COM face-specific adsorption motif in OPN and delineated separate roles for carboxylate and phosphate groups in inhibition of crystal growth by mineral-associated phosphoproteins. We propose that the formation of close-range, stable, and face-specific interactions is a key factor in the ability of phosphoproteins to regulate biomineralization processes.

Introduction

Interactions between proteins and crystals are thought to be of great importance in many, if not all, forms of biomineralization. Such interactions have been proposed to be responsible for the nucleation of crystals in mineralizing tissues,[1] the inhibition of crystallization in soft tissues,[2] formation of particular crystalline polymorphs,[3] and biological control over crystal orientation,[4] growth habit,[5] and texture.[6] Because of their unique ability to control many aspects of crystal formation, proteins are increasingly being used in nanotechnology to produce materials with desirable mechanical, optical, electrical, and other properties.[7−10]

A well-characterized crystal-modulating protein is osteopontin (OPN), which is abundant in bone and eggshell, as well as many soft tissues.[11] Upregulation of OPN gene expression has been reported in ectopic calcifications such as atherosclerotic plaque, which contain hydroxyapatite (HA),[12] and kidney stones, which most commonly contain calcium oxalate monohydrate (COM).[13] *In vitro*, OPN has been shown to inhibit the formation of HA,[14,15] calcite,[16] and COM[17,18] crystals. Studies on genetically

† CIHR Group in Skeletal Development and Remodeling and School of Dentistry.

‡ Department of Biochemistry.

§ Department of Anatomy and Cell Biology.

∥ Department of Applied Mathematics.

⊥ Present address: Faculty of Dentistry, University of British Columbia, Vancouver, Canada.

(1) Hunter, G. K.; Goldberg, H. A. *Proc. Natl. Acad. Sci. U.S.A.* **1993**, *90*, 8562−8565.
(2) Luo, G.; Ducy, P.; McKee, M. D.; Pinero, G. J.; Loyer, E.; Behringer, R. R.; Karsenty, G. *Nature* **1997**, *386*, 78−81.
(3) Falini, G.; Albeck, S.; Weiner, S.; Addadi, L. *Science* **1996**, *271*, 67−69.
(4) Belcher, A. M.; Wu, X. H.; Christensen, R. J.; Hansma, P. K.; Stucky, G. D.; Morse, D. E. *Nature* **1996**, *381*, 56−58.
(5) DeOliveira, D. B.; Laursen, R. A. *J. Am. Chem. Soc.* **1997**, *119*, 10627−10631.
(6) Berman, A.; Hanson, J.; Leiserowitz, L.; Koetzle, T. F.; Weiner, S.; Addadi, L. *Science* **1993**, *259*, 776−779.
(7) Hartgerink, J. D.; Beniash, E.; Stupp, S. I. *Science* **2001**, *294*, 1684−1688.
(8) Aizenberg, J.; Muller, D. A.; Grazul, J. L.; Hamann, D. R. *Science* **2003**, *299*, 1205−1208.
(9) Sarikaya, M.; Tamerler, C.; Jen, A. K.; Schulten, K.; Baneyx, F. *Nat. Mater.* **2003**, *2*, 577−585.
(10) Lee, S. Y.; Royston, E.; Culver, J. N.; Harris, M. T. *Nanotechnology* **2005**, *16*, S435−S441.
(11) Sodek, J.; Ganss, B.; McKee, M. D. *Crit. Rev. Oral Biol. Med.* **2000**, *11*, 279−303.
(12) Shanahan, C. M.; Cary, N. R. B.; Metcalfe, J. C.; Weissberg, P. L. *J. Clin. Invest.* **1994**, *93*, 2393−2402.
(13) Kohri, K.; Nomura, S.; Kitamura, Y.; Nagata, T.; Yoshioka, K.; Iguchi, M.; Yamate, T.; Umekawa, T.; Suzuki, Y.; Sinohara, H.; Kurita, T. *J. Biol. Chem.* **1993**, *268*, 15180−15184.
(14) Boskey, A. L.; Maresca, M.; Ullrich, W.; Doty, S. B.; Butler, W. T.; Prince, C. W. *Bone Miner.* **1993**, *22*, 147−159.
(15) Hunter, G. K.; Kyle, C. L.; Goldberg, H. A. *Biochem. J.* **1994**, *300*, 723−728.
(16) Hincke, M. T.; St. Maurice, M. In *Chemical Biology of Mineralized Tissues*; Goldberg, M., Boskey, A., Robinson, C., Eds.; American Academy of Orthopaedic Surgeons: Rosemont, Illinois, 2000; pp 13−17.

modified mice have led to the proposal that OPN is an inducible inhibitor of soft-tissue calcification.[19,20]

The inhibition of crystal formation by OPN is thought to involve an interaction between specific amino acids of the protein and an array of lattice ions on the surface of the crystal. However, as in the case of other forms of protein−crystal interaction, the amino acids and lattice ions are not known. OPN has high contents of aspartic and glutamic acids and undergoes extensive post-translation modification.[11] Bovine milk OPN has 28 sites of phosphorylation and 3 O-linked oligosaccharides;[21] rat bone OPN has at least 29 phosphorylation sites, 4 O-linked oligosaccharides, and 1 site of sulfation.[22] It has been firmly established that phosphate groups present in OPN are required for efficient inhibition of HA, calcite, or COM formation.[15,16,23−25] It has also been shown that peptides corresponding to sequences 41−52 and 290−301 of rat bone OPN are approximately 4 times more potent inhibitors of HA nucleation than sequences 7−17 and 248−264.[24]

The little information available on the OPN-binding site of crystals has mostly come from studies on COM. Using atomic force microscopy (AFM), Qiu and co-workers showed that kidney OPN decreased the rate of movement of steps (sites of rapid ion deposition) on {010} faces but not on {100} faces, a difference attributed to the greater height of the former.[26] However, Sheng and co-workers reported that milk OPN increases the adhesion between carboxylate-modified AFM tips and {100} faces of COM, suggesting a specific interaction with that face.[27,28]

We have recently characterized the OPN−COM interaction using scanning confocal and scanning electron microscopy.[29] By adding fluorescence-tagged OPN to preformed COM crystal and using He/Ne (red) and Kr/Ar (green) lasers to image the crystal and protein, respectively, we showed that rat bone OPN adsorbs preferentially to edges between {100} and {121} faces. Growth of COM in the presence of OPN resulted in a "dumbbell"-shaped crystal with concave {100} faces and rounded edges. More recently, we have found that increasing the OPN concentration results in adsorption to {100} faces and, to a lesser extent, {010} and {121} faces (Grohe, B.; O'Young, J.; Goldberg, H. A.; Hunter, G. K. Unpublished).

In the present study, we have examined the interaction between COM crystals and a synthetic peptide corresponding to residues 220−235 of rat bone OPN. This sequence contains 3 of the 29 sites of phosphorylation (serines 220, 223, and 232) identified in OPN from rat bone[22] and is one of several multiphosphorylated, aspartic/glutamic acid-rich sequences. To investigate the role of phosphorylation in interactions with COM, this peptide was synthesized in forms containing 0, 1, or all 3 phosphate groups (P0, P1, and P3).

The interaction between these peptides and COM crystals was studied using a novel combination of physical and theoretical techniques: scanning confocal microscopy to determine the crystal face(s) with which the peptides interact; scanning electron microscopy (SEM) to characterize their effects on growth habit (crystal size and shape); and atomic-level molecular dynamics (MD) simulations to determine the chemical groups involved in the interaction. These studies provide the first information about the roles of phosphate and carboxylate groups in a phosphoprotein−biomineral interaction.

Experimental Procedures

Phosphopeptide Synthesis and Labeling. Phosphopeptides were manually synthesized with free amino and carboxy termini using Fmoc chemistry as previously described[24] and purified by high-performance liquid chromatography on a C18 column. Final peptide preparations were >98% pure. From electrospray mass spectrometry, the following masses were obtained (theoretical values in parentheses): P0, 1733.7 (1733.7); P1, 1813.3 (1814.7); P3, 1975.9 (1974.7). Labeling of the peptides with AlexaFluor-488, which reacts with primary amines, was performed as previously described,[29] except that dialysis tubing with a nominal cutoff of 1 kDa was used (SpectraPor). Following dialysis, recovery of peptide was determined by amino acid analysis (Alberta Peptide Institute, Edmonton, Canada).

Crystallization Experiments and Imaging. Crystallization of COM was initiated using the method previously described.[29] Final concentrations were 1 mM calcium nitrate, 1 mM sodium oxalate, 10 mM sodium acetate, and 150 mM sodium chloride. SEM and confocal imaging were performed as previously described.[29] Confocal images were imported into Photoshop 7.0 (Adobe), and the red and green channels separated. The green-channel images were transformed into greyscale images but not modified further. SEM images were imported into CorelDRAW X3 (Corel Corporation), cropped, and indexed, and the final images were exported as bitmaps. All images reported here are raw unfiltered data.

Molecular Dynamics. Atomic scale MD simulations were performed using the GROMACS suite.[30] For force field, we used GROMOS96 version 45A3, which has proven to be a reliable description for lipids, peptides, and other biomolecules.[31] The coordinates for the COM {100} face were taken from previously obtained experimental results.[32] The topology for oxalate was generated using PRODRG.[33] Extended conformations were used as the initial peptide structure. For each simulation, peptides were oriented parallel to the crystal surface where the center of mass difference between the crystal slab and the peptide was approximately 4 nm in the direction perpendicular to the surface. The crystal slab was placed at the center of the periodic cell and constructed to be approximately 0.7 nm thick with the Ca^{2+} dense layers of the {100} face exposed on each side. Periodic boundary conditions were applied with the size of the simulation cell being 8.7 nm × 6.2

(17) Shiraga, H.; Min, W.; VanDusen, W. J.; Clayman, M. D.; Miner, D.; Terrell, C. H.; Sherbotie, J. R.; Foreman, J. W.; Przysiecki, C.; Nielson, E. G.; Hoyer, J. R. *Proc. Natl. Acad. Sci. U.S.A.* **1992**, *89*, 426−430.
(18) Worcester, E. M.; Blumenthal, S. S.; Beshensky, A. M.; Lewand, D. L. *J. Bone Miner. Res.* **1992**, *7*, 1029−1036.
(19) Speer, M. Y.; McKee, M. D.; Guldberg, R. E.; Liaw, L.; Yang, H. Y.; Tung, E.; Karsenty, G.; Giachelli, C. M. *J. Exp. Med.* **2002**, *196*, 1047−1055.
(20) Mo, L.; Huang, H. Y.; Zhu, X. H.; Shapiro, E.; Hasty, D. L.; Wu, X. R. *Kidney Int.* **2004**, *66*, 1159−1166.
(21) Sørensen, E. S.; Højrup, P.; Petersen, T. E. *Protein Sci.* **1995**, *4*, 2040−2049.
(22) Keykhosravani, M.; Doherty-Kirby, A.; Zhang, C.; Brewer, D.; Goldberg, H. A.; Hunter, G. K.; Lajoie, G. *Biochemistry* **2005**, *44*, 6990−7003.
(23) Jono, S.; Peinado, C.; Giachelli, C. M. *J. Biol. Chem.* **2000**, *275*, 20197−20203.
(24) Pampena, D. A.; Robertson, K. A.; Litvinova, O.; Lajoie, G.; Goldberg, H. A.; Hunter, G. K. *Biochem. J.* **2004**, *378*, 1083−1087.
(25) Hoyer, J. R.; Asplin, J. R.; Otvos, L. *Kidney Int.* **2001**, *60*, 77−82.
(26) Qiu, S. R.; Wierzbicki, A.; Orme, C. A.; Cody, A. M.; Hoyer, J. R.; Nancollas, G. H.; Zepeda, S.; De Yoreo, J. J. *Proc. Natl. Acad. Sci. U.S.A.* **2004**, *101*, 1811−1815.
(27) Sheng, X.; Ward, M. D.; Wesson, J. A. *J. Am. Chem. Soc.* **2003**, *125*, 2854−2855.
(28) Sheng, X.; Jung, T.; Wesson, J. A.; Ward, M. D. *Proc. Natl. Acad. Sci. U.S.A.* **2005**, *102*, 267−272.
(29) Taller, A.; Grohe, B.; Rogers, K.; Goldberg, H. A.; Hunter, G. K. *Biophys. J.* **2007**, *93*, 1768−1777.
(30) Van Der Spoel, D.; Lindahl, E.; Hess, B.; Groenhof, G.; Mark, A. E.; Berendsen, H. J. *J. Comput. Chem.* **2005**, *26*, 1701−1718.
(31) Schuler, L. D.; Daura, X.; van Gunsteren, W. F. *J. Comput. Chem.* **2001**, *22*, 1205−1218.
(32) Tazzoli, V.; Domenghetti, C. *Am. Mineral.* **1980**, *65*, 327−334.
(33) Aalten, D. M. F.; Bywater, R.; Findlay, J. B. C.; Hendlich, M.; Hooft, R. W. W.; Vriend, G. *J. Comput.-Aided Mol. Des.* **1996**, *10*, 255−262.
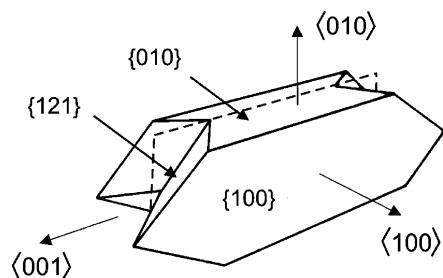
Figure 1. Faces and crystallographic directions of calcium oxalate monohydrate crystals. Broken line indicates twin plane. Reproduced from ref 29.

nm in the plane of the surface and 10 nm perpendicular to the surface. The system was solvated with simple point charge (SPC) water,[34] and Cl^- counterions were added to maintain the system charge-neutral. Prior to the actual simulation runs, energy minimization was performed without constraints using the steepest descent method.

The simulations were performed in the NVT ensemble at 300 K, and the bond lengths were constrained using the SHAKE algorithm.[35] Crystal atoms were constrained to their equilibrium positions. The Berendsen thermostat with a coupling time constant of 0.1 ps was employed, and the particle mesh Ewald method[36−38] was used for electrostatics. The time step was set to 2 fs. Systems were simulated for 50 ns each. All simulations were run in parallel over eight processors on the SHARCNET grid computing facility (www.sharcnet.ca).

Results

Figure 1 shows the growth habit of COM crystals formed under the conditions used in the present study. These are monoclinic penetration twins with {010}, {100}, and {121} faces developed. Also shown in Figure 1 are the major crystallographic directions, ⟨010⟩, ⟨100⟩, and ⟨001⟩. Note that lattice-ion addition to {010} and {100} faces results in crystal growth in ⟨010⟩ and ⟨100⟩ directions, respectively; however, ion addition to {121} faces results in growth in ⟨001⟩ directions. The ⟨010⟩ and ⟨100⟩ dimensions of a crystal represent the distance between its {010} and {100} faces, respectively. The ⟨001⟩ dimension is the largest distance between points on the crystal as measured along the ⟨001⟩ axis.

COM crystals grown in the presence of 2 or 20 µg/mL P0 (SHESTEQSDAIDSAEK), P1 (SHESTEQSDAIDpSAEK), or P3 (pSHEpSTEQSDAIDpSAEK), or no peptide, were visualized by SEM. Dramatic effects on crystal growth habit were observed, including inhibition of growth in ⟨100⟩ directions and, in the case of P3, rounding of edges and apparent loss of {010} faces (Figure 2). To quantify these effects, the ⟨001⟩, ⟨010⟩, and ⟨100⟩ dimensions of crystals were measured. From these measurements and the numbers of crystals present, total volumes of precipitate were also estimated (Table 1). At 2 µg/mL, P0 increased COM size in all three dimensions. There was no increase in total crystal volume, indicating that fewer crystals were nucleated. 20 µg/mL P0 had no significant effect on crystal size or total crystal volume. The effects of 2 and 20 µg/mL P1, as well as 2 µg/mL P3, were qualitatively similar: the ⟨100⟩
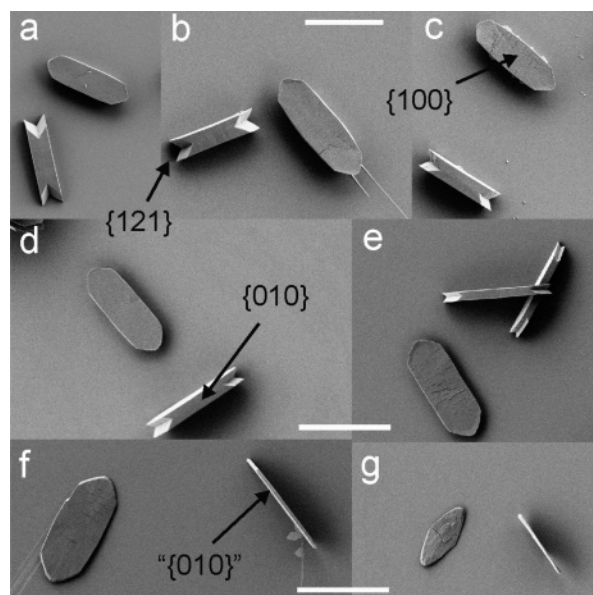
Figure 2. Effects of peptides on growth habit of COM crystals. COM crystals were grown in the presence of P0, P1, P3, or no peptide and imaged by SEM. All scale bars are 11 µm. Scale bar in panel b also applies to panels a and c. (a) No peptide; (b) P0, 2 µg/mL; (c) P0, 20 µg/mL; (d) P1, 2 µg/mL; (e) P1, 20 µg/mL; (f) P3, 2 µg/mL; (g) P3, 20 µg/mL.

dimension was decreased, while the ⟨010⟩ dimension was increased. At 20 µg/mL P1 or 2 µg/mL P3, the total volume was decreased. P3 had the most significant effects on formation of COM crystals, decreasing the ⟨100⟩ dimension more at 2 µg/ mL (54%) than P1 did at 20 µg/mL (38%). At 20 µg/mL, P3 caused significant inhibition of growth in ⟨001⟩ (33%) and ⟨010⟩ (13%) as well as ⟨100⟩ (64%) directions and decreased the total crystal volume by 94%. The main findings are therefore that P1 and P3 both inhibit COM growth in ⟨100⟩ directions; at higher concentrations, P3 also inhibits growth in ⟨001⟩ and ⟨010⟩ directions.

To identify the faces of COM with which OPN220−235 interacts, aliquots of each peptide were labeled with AlexaFluor-488 and added to solutions in which COM crystals had been grown. Images were collected with He/Ne (red) and Kr/Ar (green) lasers every 0.5−1.0 µm along the microscopic *z*-axis. Each image shown in Figure 3 is an optical section taken approximately halfway along the ⟨010⟩ dimension of a crystal nucleated from a {010} face. The perimeters of such sections consist of two {100} side faces and four {121} end faces. For all three peptides, fluorescence was observed mainly on {100} faces of the crystal. In the case of P0 and P3, some fluorescence was also associated with {121} faces. The intensity of fluorescence on {100} faces was greater with P1 and P3 than with P0, suggesting that the former peptides may adsorb more strongly. However, these intensity differences may also reflect variations between the peptides in efficiency of conjugation with the fluorochrome. Examination of crystals nucleated from a {100} face showed that P0, P1, or P3 did not adsorb significantly to {010} faces (Figure 4).

To investigate the mechanism of adsorption, we performed the first atomic-scale molecular-dynamics simulation of a protein−crystal interaction. Simulated peptides in an extended conformation were placed 4 nm from and parallel to a section of the {100} face, and the system was allowed to evolve for 50 ns. Image sequences show that the three peptides behave very

(34) Berendsen, H. J. C.; Postma, J. P. M.; van Gunsteren, W. F.; Hermans, J. In *Intermolecular Forces*; Pullman, B., Ed.; Reidel: Dordrecht, Netherlands, 1981.
(35) Ryckaert, J. P.; Ciccotti, G.; Berendsen, H. J. C. *J. Comput. Phys.* **1977**, *23*, 327−342.
(36) Smith, P. E.; Pettitt, B. M. *J. Chem. Phys.* **1991**, *95*, 8430−8441.
(37) Patra, M.; Karttunen, M.; Hyvonen, M. T.; Lindqvist, P.; Falck, E.; Vattulainen, I. *Biophys. J.* **2003**, *84*, 3636−3645.
(38) Essman, U.; Perela, L.; Berkowitz, M. L.; Darden, T.; Lee, H.; Pedersen, L. G. *J. Chem. Phys.* **1995**, *103*, 8577−8592.

Table 1. Effects of Osteopontin Peptides on COM Crystal Dimensions[a]

peptide	concn (μg/mL)	$\langle 001 \rangle$ dimension (μm)	$\langle 010 \rangle$ dimension (μm)	$\langle 100 \rangle$ dimension (μm)	volume of precipitate (μm^3/mm^2)
–	–	13.60 ± 2.04 (67)	3.98 ± 0.70(86)	3.06 ± 0.65(53)	49,188 ± 12,867(8)
P0	2	14.60 ± 2.52(54)[b]	4.89 ± 0.69(30)[b]	3.65 ± 0.83(24)[c]	35,796 ± 6,426(5)
P0	20	13.0 ± 1.93 (47)	4.32 ± 0.55 (28)	2.86 ± 0.56 (19)	49,354 ± 3,780(3)
P1	2	12.80 ± 2.48(107)	4.47 ± 0.69(67)[c]	2.36 ± 0.74(40)[c]	48,968 ± 13,568(6)
P1	20	13.10 ± 1.81(74)	4.92 ± 0.70(44)[c]	1.89 ± 0.52(30)[c]	22,108 ± 7,838(4)[c]
P3	2	13.80 ± 2.28(47)	5.25 ± 0.94(29)[c]	1.42 ± 0.51(18)[c]	11,665 ± 4,035(5)[c]
P3	20	9.06 ± 0.96(33)[c]	3.48 ± 0.52(22)[b]	1.11 ± 0.00(11)[c]	1,932 ± 725(3)[c]

[a] $\langle 001 \rangle$ and $\langle 010 \rangle$ dimensions were measured from scanning electron micrographs of COM crystals nucleated from {100} faces, $\langle 001 \rangle$ and $\langle 100 \rangle$ dimensions from crystals nucleated from {010} faces. Volumes of precipitate were calculated as follows: mean area of the {100} face × mean $\langle 100 \rangle$ dimension × number of crystals/mm^2. Values given are mean ± standard deviation, with numbers of replicates in parenthesis (for volumes, n = number of microscopic fields). [b] $P < 0.05$. [c] $P < 0.01$ − significantly different from corresponding control (Dunnett's multiple comparison test).
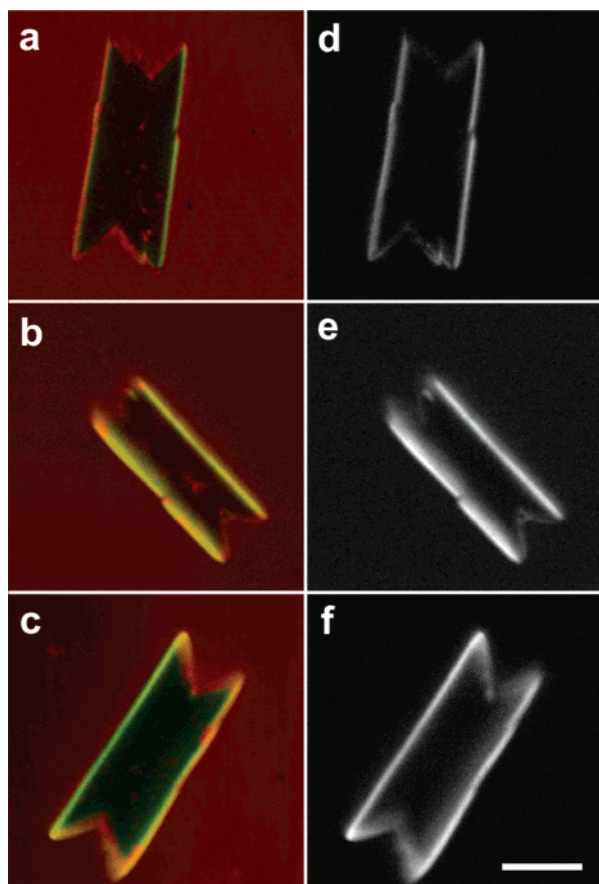
Figure 3. Adsorption of Alexa-labeled peptides to COM crystals nucleated from {010} faces. Images shown are optical sections taken approximately halfway through the thickness of the crystals. Panels a, b, and c are combined red (crystal) and green (peptide) channel images; panels d, e, and f are green channel images converted to greyscale. (a, d) P0, 0.2 μg/mL; (b, e) P1, 0.2 μg/mL; (c, f) P3, 0.2 μg/mL.

Figure 4. Adsorption of Alexa-labeled peptide P3 to COM crystal nucleated from a {100} face. Panels a and b are red-green images; panels c and d are green-channel images converted to greyscale. Images in panels a and c are optical sections through the upper surface of the crystal, showing intense labeling of the {100} face. Images in panels b and d are optical sections taken midway through the thickness of the crystal, showing labeling of {121} (end) faces and lack of labeling of {010} (side) faces.

differently (see Supporting Information). P3 rapidly forms multiple stable contacts with the {100} face, although noninteracting side chains still exhibit considerable motion. P1 adsorbs much more slowly, with initial single contacts near the N- and C-termini gradually increasing in number; unlike P3, a central region of the peptide remains relatively distant and highly mobile. P0 forms one or two stable contacts at its C-terminal end, but the rest of the peptide is unable to adsorb. "Snapshots" of P0, P1, and P3 taken at 20 ns are shown in Figure 5.
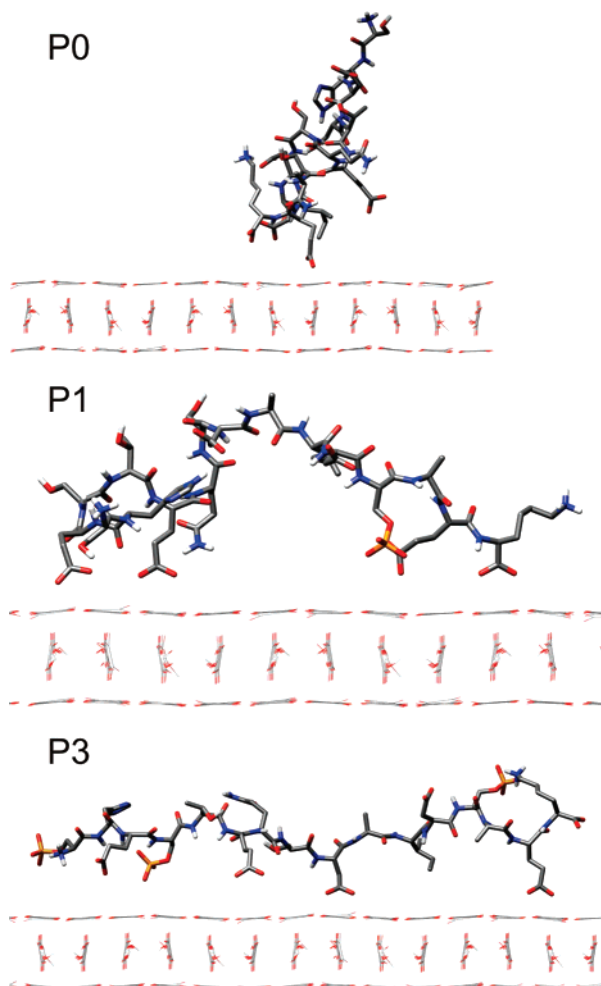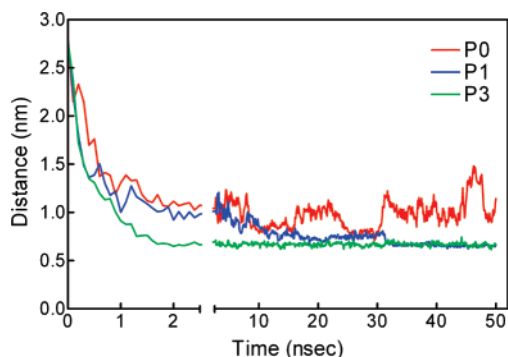
To quantify these interactions, the distance of the peptide center of mass from the top layer of crystal atoms was plotted against simulation time (Figure 6). By 2−3 ns, P3 had reached its position closest to the {100} face, and this distance fluctuated

very little throughout the remainder of the simulation. P1 came into close contact with the crystal more slowly, but by 30 s its distance from the face was similar to that of P3. P0 did not achieve as close a contact as P3 or P1, and its distance from the face exhibited large fluctuations. For each peptide, the distance of the center of mass from the crystal surface was averaged over the period 5−50 ns. These distances were (mean ± standard deviation) 0.975 ± 0.145 nm for P0, 0.732 ± 0.081 nm for P1, and 0.668 ± 0.0184 nm for P3. All these values are significantly different from one another ($P < 0.001$, Dunn's multiple comparison test).

To identify the amino acids involved in the interaction between OPN220−235 and the {100} face of COM, the average distances between side-chain center of mass and the crystal surface over the period of 5−50 ns were calculated (Figure 7a). P0 interacted with the crystal only at its C-terminal end. The residues closest to the face were carboxylate-bearing residues at or near the C-terminus: D12, E15, and K16. P1 formed close contacts at both its N-terminal (E3, E6) and C-terminal (pS13, E15, K16) ends, but the central part of the molecule (Q7-D12) was relatively distant (≥ 0.7 nm) from the face. For P3, the mean
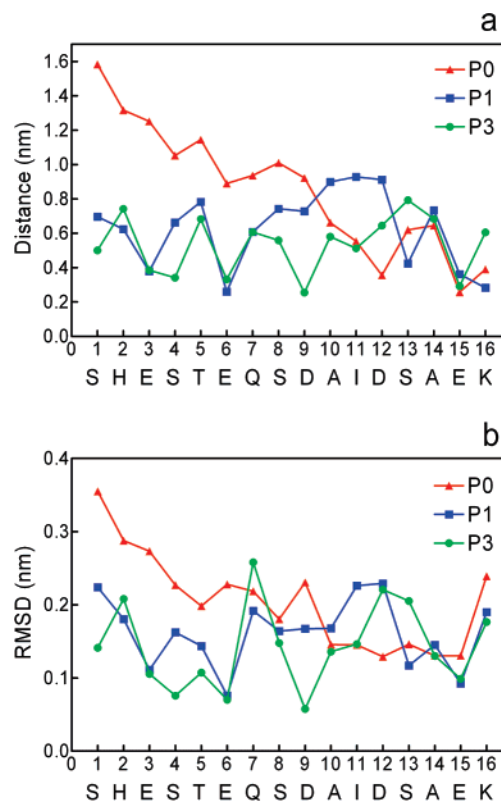
Figure 5. Peptide positions at 20 ns of simulation. Peptide: C - gray, H - white, O - red, N - blue, P - orange.

Figure 6. Molecular-dynamics simulations of peptide adsorption to {100} face of COM: peptide center-of-mass calculations. For each peptide, the vertical distance between the center of mass of the peptide and the surface layer of crystal atoms was measured every 0.1 ns between 5 and 50 ns and averaged.

Figure 7. Molecular-dynamics simulations of peptide adsorption to {100} face of COM: amino acid center-of-mass calculations. (a) The vertical distance between the center of mass of each side chain and the surface layer of crystal atoms was measured every 0.1 ns between 5 and 50 ns and averaged. (b) The root-mean-square deviation in the position of each side-chain center of mass (in any direction) over the period 5−50 ns was calculated.

face exhibit little fluctuation. Note, however, that the N- and C-terminal residues are particularly mobile (except when the former is phosphorylated), as is Q7.

Discussion

It is well-established that substances adsorbing to a crystal face will inhibit subsequent growth of that face; that is, a protein interacting with {*hkl*} faces will inhibit growth in ⟨*hkl*⟩ directions.[39] In agreement with this, we showed by confocal imaging of fluorescence-labeled peptides that P1 and P3 adsorb preferentially to {100} faces of COM and by SEM that both these peptides inhibit growth in ⟨100⟩ directions. Compared to the other faces developed, {010} and {121}, the {100} face is relatively rich in Ca^{2+} ions; this fact may well explain its affinity for an acidic sequence such as OPN220−235, which contains aspartic or glutamic acid at every third position. Also consistent with the prevailing paradigm of protein−crystal interaction is our observation that P3 adsorbs to {121} faces of COM and inhibits crystal growth in ⟨001⟩ directions.

However, certain findings of our study are in apparent disagreement with the paradigm. Notably, although both P1 and P3 adsorb strongly to {100} faces of COM, P3 is a much more effective inhibitor of ⟨100⟩ direction growth. An explanation for these apparent discrepancies comes from our MD analyses. These show that P3 adsorbs to the {100} face of COM in such a manner that its center of mass is significantly closer to the

distances of all residues were quite similar, indicating that this peptide interacts with the crystal throughout its sequence. The amino acids of P3 in closest contact were E3, pS4, E6, D9, and E15. Interestingly, pS13 was the residue most distant from the crystal face.

The average root-mean-square distances (rmsd's) of side-chain atoms were also calculated (Figure 7b). A low average rmsd for an amino acid indicates that its position varies relatively little with time. In general, amino acids located close to the

(39) Addadi, L.; Weiner, S. *Proc. Natl. Acad. Sci. U.S.A.* **1985**, *82*, 4110−4114.

surface atoms of the crystal face than that of P1. Also, the position of P3 relative to the face exhibits less variation. This finding provides an important qualification to the principle mentioned above: *only peptides or proteins able to achieve a sufficiently close and stable interaction with a crystal face will effectively inhibit growth of that face*.

The inhibition of $\langle 100 \rangle$-direction growth by P1 or by 2 μg/ mL P3 is associated with increases in $\langle 010 \rangle$-direction growth. The obvious interpretation is that adsorption of peptide to one set of faces allows other faces to grow more rapidly, as we have previously observed in the inhibition of crystal growth by poly-L-aspartic acid.[40] Growth of noninteracting faces may also be increased by decreases in nucleation rate, although this has not been fully analyzed in the present study.

Previous molecular-modeling studies of protein−crystal interactions have generally assumed that some part of the protein folds into a conformation that is stereochemically complementary to a crystal face. For example, the γ-carboxyglutamic acid residues in an α-helical region of osteocalcin were shown to be spaced appropriately to interact with Ca^{2+} ions on the {001} lattice planes of HA.[41,42] Similar approaches were used to model the adsorption of an antifreeze protein to the (2021) plane of ice crystals[43] and dentin phosphophoryn to {010} planes of octacalcium phosphate.[44] However, several mineral-binding proteins, including OPN,[45] bone sialoprotein,[46,47] and the mollusk-shell protein lustrin[48] are largely or entirely devoid of folded structure. Our simulations show that P0, P1, and P3 do not adopt a stable conformation prior to interaction with the {100} face; rather, these peptides exhibit a considerable degree of molecular diffusion and bond rotation in order to achieve a stable set of electrostatic contacts. This is in agreement with a previous study on the interaction of the N-terminal peptide of lithostathine with the calcite crystal.[49]

MD simulations have become an invaluable tool in studies of biomolecular systems.[50] In the present case, the degree of agreement with our physical studies provides reassurance about the robustness of the MD analyses. Specifically, there is an excellent inverse correlation between the predicted peptide center-of-mass distance from the {100} face (P0 [0.975 nm] > P1 [0.732 nm] > P3 [0.668 nm]) and the degree of inhibition of $\langle 100 \rangle$-direction growth (at 20 μg/mL, P0 [0%] < P1 [38%] < P3 [64%]). Thus, the more closely a peptide associates with the {100} face, the better it inhibits crystal growth perpendicular to that face. We have also been able to identify which amino acids of OPN220−235 are involved in the interaction of the peptide with the {100} face. The phosphoserines present in P1 and P3 result in these peptides achieving a closer approximation to the crystal face. However, in neither P1 nor P3 is the residue

closest to the face of a phosphoserine, but rather a glutamic acid (E6) for P1 and an aspartic acid (D9) for P3. The most *distant* residue in P3 is pS13. These findings suggest that phosphate groups provide a strong negative charge that drives the peptide close to the {100} face but that carboxylate groups, perhaps for stereochemical reasons, are capable of more specific interactions with Ca^{2+} ions of the crystal. By electrostatic repulsion, phosphates may also assist the interaction by maintaining the peptide in an extended conformation.[51]

AFM studies on the inhibition of COM growth demonstrated that OPN, as well as aspartic acid, poly-aspartic acid, and aspartic acid-rich oligopeptides, affects the movement of COM crystal steps in face- and direction-specific fashions.[26,52−55] The effects of poly-aspartic acid were found to be consistent with adsorption of the polypeptide to either (021) steps on {100} faces or to the {100} faces themselves.[54] In the case of OPN, a greater inhibition of growth of the quadruple steps formed on {010} faces than the single steps formed on {100} faces was thought to indicate an interaction of the protein with the step riser as well as the base.[26] The confocal and SEM studies reported above are consistent with OPN220−235 adsorbing to steps on {100} faces rather than to the face itself. However, the MD analysis demonstrates a strong, phosphorylation-dependent interaction with the {100} lattice plane. Therefore, it is likely that if OPN220−235 inhibits step movement on the {100} face, it does so by pinning the base of the step rather than interacting with the riser.

Conclusion

We have identified a phosphorylated sequence in OPN that adsorbs preferentially to {100} faces of COM crystals. The presence of phosphate groups results in peptides achieving a closer and more stable interaction with the crystal, and consequently inhibiting crystal growth more effectively. However, it is glutamic and aspartic acid residues that form the closest contacts with Ca^{2+} ions of the {100} face. This study therefore provides an explanation for the high contents of phosphoserine and acidic amino acids found in many mineral-modulating proteins.

Supporting Information Available: Image sequences of P1, P2, and P3. This material is available free of charge via the Internet at http://pubs.acs.org.

JA0745613

(40) Grohe, B.; Rogers, K.; Goldberg, H. A.; Hunter, G. K. *J. Cryst. Growth* **2006**, *295*, 148−157.

(41) Hauschka, P. V.; Wians, F. H., Jr. *Anat. Rec.* **1989**, *224*, 180−188.

(42) Hoang, Q. Q.; Sicheri, F.; Howard, A. J.; Yang, D. S. *Nature* **2003**, *425*, 977−980.

(43) Wen, D.; Laursen, R. A. *Biophys. J.* **1992**, *63*, 1659−1662.

(44) Furedi-Milhofer, H.; Moradian-Oldak, J.; Weiner, S.; Veis, A.; Mintz, K. P.; Addadi, L. *Connect. Tissue Res.* **1994**, *30*, 251−264.

(45) Fisher, L. W.; Torchia, D. A.; Fohr, B.; Young, M. F.; Fedarko, N. S. *Biochem. Biophys. Res. Commun.* **2001**, *280*, 460−465.

(46) Wuttke, M.; Muller, S.; Nitsche, D. P.; Paulsson, M.; Hanisch, F. G.; Maurer, P. *J. Biol. Chem.* **2001**, *276*, 36839−36848.

(47) Tye, C. E.; Rattray, K. R.; Warner, K. J.; Gordon, J. A.; Sodek, J.; Hunter, G. K.; Goldberg, H. A. *J. Biol. Chem.* **2003**, *278*, 7949−7955.

(48) Wustman, B. A.; Weaver, J. C.; Morse, D. E.; Evans, J. S. *Connect. Tissue Res* **2003**, *44 Suppl 1*, 10−15.

(49) Gerbaud, V.; Pignol, D.; Loret, E.; Bertrand, J. A.; Berland, Y.; Fontecilla-Camps, J. C.; Canselier, J. P.; Gabas, N.; Verdier, J. M. *J. Biol. Chem.* **2000**, *275*, 1057−1064.

(50) Saiz, L.; Klein, M. L. *Acc. Chem. Res.* **2002**, *35*, 482−489.

(51) Forster, S.; Schmidt, M.; Antonietti, M. *J. Phys. Chem.-Us* **1992**, *96*, 4008−4014.

(52) Orme, C. A.; Noy, A.; Wierzbicki, A.; McBride, M. T.; Grantham, M.; Teng, H. H.; Dove, P. M.; DeYoreo, J. J. *Nature* **2001**, *411*, 775−779.

(53) Guo, S. W.; Ward, M. D.; Wesson, J. A. *Langmuir* **2002**, *18*, 4284−4291.

(54) Jung, T.; Sheng, X.; Choi, C. K.; Kim, W. S.; Wesson, J. A.; Ward, M. D. *Langmuir* **2004**, *20*, 8587−8596.

(55) Wang, L.; Qiu, S. R.; Zachowicz, W.; Guan, X.; Deyoreo, J. J.; Nancollas, G. H.; Hoyer, J. R. *Langmuir* **2006**, *22*, 7279−7285.